Article

Live-Cell Pyrophosphate Imaging by In-Situ Hot-Spot Generation

Mingmin Li, Jin Li, Huixia Di, Huiqiao Liu, and Dingbin Liu

Anal. Chem., **Just Accepted Manuscript** • DOI: 10.1021/acs.analchem.6b04786 • Publication Date (Web): 23 Feb 2017

Live-Cell Pyrophosphate Imaging by In-Situ Hot-Spot Generation

Mingmin Li,[†] Jin Li,[†] Huixia Di,[†] Huiqiao Liu,[†] and Dingbin Liu*[,†,‡]

[†] College of Chemistry, Research Center for Analytical Sciences, State Key Laboratory of Medicinal Chemical Biology, and Tianjin Key Laboratory of Molecular Recognition and Biosensing, Nankai University, Tianjin 300071 (China)

[‡] Collaborative Innovation Center of Chemical Science and Engineering (Tianjin), Tianjin 300071 (China)

KEYWORDS: pyrophosphate, bioimaging, surface-enhanced Raman spectroscopy, hot spot, nanoprobes

ABSTRACT: Controlling the electromagnetic hot-spot generation is essential for surface-enhanced Raman scattering (SERS) assays. Current hot spot-based SERS assays have been extensively studied in solutions or on substrates. However, probing biospecies by controlling the hot-spot assembly in living systems has not been demonstrated thus far. Herein, we report a background-free SERS probe for imaging pyrophosphate (PPi), a biochemically significant anion, in living cells. Intracellular PPi is able to induce the nanoparticle dimerization, thus creating an intense electromagnetic hot spot and dramatically enhancing the signal of the Raman reporters residing in the hot spot. More impressively, the reporter we used in this study provides a strong and sharp single peak in the cellular Raman-silent region (1800-2800 cm^{-1}), thus eliminating the possible background interference. This strategy could be readily extended to detect other biomarkers by only replacing the recognition ligands.

INTRODUCTION

Probing anions in living cells could open an exciting window for better understanding of diverse pathophysiologically relevant events. Pyrophosphate (PPi), the product of adenosine triphosphate (ATP) hydrolysis in cells, is tightly associated with a wide range of biologically significant processes such as information processing and energy transduction.[1,2] The detection of PPi release can provide valuable information on identifying several diseases including chondrocalcinosis or calcium pyrophosphate dehydrate crystal deposition, Monckeberg's arteriosclerosis, and even cancers.[3-5] Considering its importance, a major thrust in the past two decades has been the development of high-performance probes for PPi and its derivatives.[6-11] Among these, fluorescent chemosensors based on metal coordination are highly attractive owing to their high sensitivity and selectivity, fast response,[10-14] and the capability of live-cell imaging.[15-17] However, these fluorescent probes are facing several key issues such as photobleaching, background autofluorescence, self-quenching, and poor water-solubility for a majority of the dyes.[18-20] These issues impede the precise detection of PPi in aqueous solutions especially in living systems.

Realizing the above issues, there is an increasing incentive to find alternative means for in situ probing PPi in living cells. Surface-enhanced Raman scattering (SERS) is gaining considerable attention in a number of chemical and biomedical applications owing to its distinct properties including high sensitivity, high multiplicity, rich molecular information, and resistance to photobleaching.[21-23] Particularly, single-molecule sensitivity can be achieved by residing the analytes in the hot spots of metal nanostructures.[24] However, the reproducibility of SERS signals is poor because the hot spots are rare (<0.1% of the total Raman-active sites) and their distribution is random.[25] The poor signal reproducibility limits the practical applications of the hot spot-based SERS probes especially in complex samples. In recent years, enormous efforts have been devoted to the fabrication of structurally reproducible nanoprobes with uniform hot spots.[26,27] Despite that numerous hot spot-based SERS assays have been employed to detect compounds in solutions or on substrates, it thus far remains a major challenge to monitor biospecies in living systems by in situ controlling the hot-spot assembly.

We herein propose a strategy for imaging PPi in living cells with high sensitivity and selectivity, and simultaneously with nearly zero background interference. This strategy is based on the specific PPi-triggered dimerization of gold nanoparticles (AuNPs), which leads to the in-situ formation of hot spots and thus markedly enhances the Raman intensity of the reporters (**Scheme 1**). Compared with conventional SERS substrates whose hot spots have already been made prior to analysis, our SERS probe produces hot spots only in the presence of analytes. It is worth noting that we design asymmetrically functionalized PEGylated AuNPs as the aqueous SERS substrates, by which uniform AuNP dimers could be produced and the PPi is thus sandwiched in the typical gapped hot spots. The specific AuNP dimerization is ascribed to the strong metal coordination interaction between PPi and the bis(2-pyridylmethyl)amine (DPA)-Zn^{2+} complex anchored on the AuNP surfaces. Combination of the uniform gapped hot spots and the high probe affinity ensures high reproducibility of the SERS probes in both aqueous solutions and living cells. More significantly, we employ 4-mercaptobenzonitrile (MBN) as the reporter, which shows a strong and sharp single peak in the cellular Raman-silent region (1800-2800 cm^{-1}) of the Raman spectrum,[28] where the intracellular endogenous species (such as proteins and lipids) do not show any Raman signals, thus eliminating background interference.[29-31] Ultimately, three-dimensional (3D) imaging technique was employed to map the enhanced background-free Raman signals and thus the distribution of PPi in living cells.

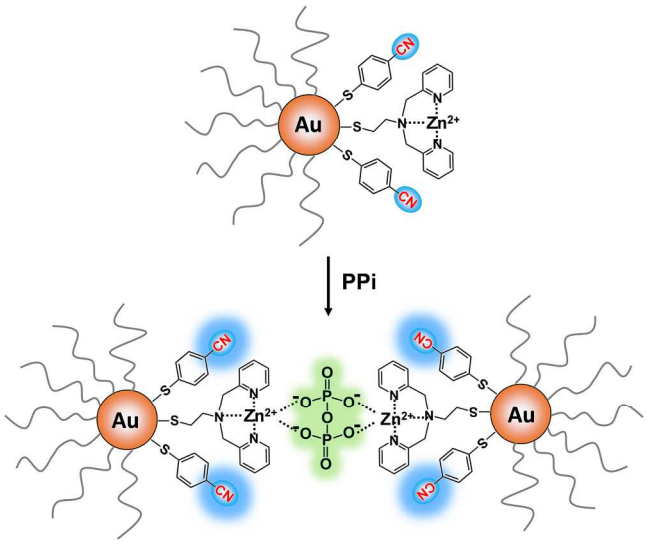

Scheme 1. Schematic illustration of AuNP dimerization through the PPi-mediated metal coordination. An electromagnetic hot spot is formed in the dimer and the background-free Raman signal of nitriles could be markedly enhanced.

EXPERIMENTAL SECTION

Materials and instrumentation. 2,2'-Dipicolylamine (DPA) was purchased from Huateng (Hunan, China). Ethylene sulfide was purchased from Heowns (Tianjin, China). HS-PEG-OCH_3 (MW 2000) was obtained from Sigma Aldrich (St. Louis, USA). Gold (III) chloride trihydrate ($HAuCl_4 \cdot 3H_2O$), hydroxylammonium chloride, 4-mercaptobenzonitrile (MBN), sodium pyrophosphates, (3-aminopropyl) triethoxysilane (APTES), and zinc nitrate hexahydrate were purchased from Aladdin (Shanghai, China). Tri-sodium citrate was purchased from Alfa Aesar (Tianjin, China). Ethyl acetate and 2-propanol were purchased from Concord (Tianjin, China). De-ionized water (Milli-Q grade, Millipore) with a resistivity of 18.2 MΩ·cm was used throughout the experiment. ^{1}H NMR spectrum was recorded by a Varian 400 MHz spectrometer. JMS-LC mate mass spectrometer was applied to record electron spray ionization mass spectra (ESI-MS). Hitachi U-3900 UV-vis spectrophotometer was used to record the absorption spectra of AuNP solutions. Synergy 2 Multi-Mode Microplate Reader (Bio-Tek Instruments, Inc.) was used to record the absorbance of AuNPs in 96-well plates. JEOL 1400 model at an accelerating voltage of 100 kV was applied to keep track of TEM images this study. The Raman spectra and cell imaging were collected on a Renishaw in Via Raman microscope. The Raman spectra of solutions were measured in capillaries with average length of 10 cm and diameter of 0.5 mm. 633-nm laser was adopted for sample excitation in all the related experiments.

Synthesis of N-(2-mercaptoethyl)-di(2-pyridymethyl)amine (DPASH). DPASH was synthesized according to the literature,[32] as illustrated in **Scheme S1** in Supporting Information. In brief, 2, 2'-dipicolylamine (2.8 mL, 15.6 mmol) in dry toluene (3.1 mL) was placed in a round-bottom flask. Subsequently, ethylene sulfide (1.65 mL, 31.2 mmol) in toluene (3.1 mL) was added dropwise and the mixture was mildly stirred for 2 days. The resulting solution was evaporated under reduced pressure and the impurities were removed by column chromatography with silica gel (eluent, AcOEt: i-PrOH=20:1, $NH_3 \cdot H_2O$ 5%). Then, the excess solvent was removed in vacuo to give DPASH as a yellow oil in 43% yield.

Preparation of citrate-capped AuNPs (30 nm in diameter). The 30 nm AuNPs with a narrow size distribution was prepared through reduction of chloroauric acid with hydroxylamine hydrochloride, as proposed by Turkevich in 1951.[33] Briefly, hydroxylamine hydrochloride (0.4 mM, 1 mL) was quickly added to the 13 nm sized AuNPs (0.196 nM, 125 mL) solution, and then an aqueous solution of $HAuCl_4$ (100 mM) in 10 mL water was added dropwise with vigorous stirring for another 30 min. Finally, 1.6 mL of the 10% w/w tri-sodium citrate solution was added into the above solution and the mixture was stirred for another 15 minutes. The resulted solution was characterized by UV–vis spectroscopy and its maximal absorption band is at about ~525 nm.

Simulation of the electric field distributions. The simulation of the electric field distributions on AuNPs is performed by COMSOL Multiphysics software with the RF module. For mono-dispersed AuNPs, we set the diameter as 30 nm, for the dimer, the distance between two AuNPs was set to be 1 nm-consisting with the molecular size of DPASH, and the same diameter with mono-dispersed AuNPs. We put the configuration into liquid which has a refractive index of 1.33. The AuNPs were irradiated by an incident plane wave, whose electric-field polarization was matching the ligature between the two particles' centers. Numbers in the scale bar of the contrast represent the intensity of $|E|/|E_{inc}|$, reflecting the normalized near-field distribution, where E and E_{inc} are the electric vectors of the total field and incident plane wave, respectively.

Preparation of the AuNP dimer probes. Glass slides with a dimension of 22 mm × 22 mm were used to fabricate the AuNP dimer probes. Glass coverslips were firstly cleaned by immersing them into piranha solution (sulfuric acid: hydrogen peroxide=3:1) for 30 min at room temperature. (Piranha is a vigorous oxidant and should be used with extreme caution). Then the substrates were sonicated in pure water for 3×20 min, followed by sonicated in ethanol for 3×20 min, then immersed into ethanol for further use. For modification procedure, as illustrated in **Scheme S2** in Supporting Information, the clean glass slides were treated with 10% w/w APTES solution for 30 min to produce amino groups. Further sonication was allowed to remove the free APTES. The glass substrates were immersed into the previously prepared AuNPs solution (2 mL) overnight and then rinsed with water. The fixed AuNPs were incubated with the mixture of 7 μM DPASH and 3 μM MBN in 2 mL ethanol solution for 30 min, enabling DPASH and MBN to attach onto the exposed area of the AuNPs through Au-S chemical bonds. Then, the slides were immersed into 1 mL $Zn(NO_3)_2$ (10.5 μM) solution for 2 h at room temperature. Zn^{2+} binds to DPASH though the specific complexation. The three nitrogens of a DPA ligand can coordinate strongly to a Zn^{2+} cation with an association constant around 10^7 M^{-1} in water [12] and the association constant (K_a) for PPi and bis(Zn^{2+}-dipicolylamine) was determined to be 10^5-10^8 M^{-1} [14,16]. Finally, the other side of AuNP surfaces was modified with PEG (MW 2000) by sonicating into 1 mL HS-PEG solution (10 μM) supplemented with 0.5% SDS, thus making AuNPs asymmetrically decorated. The excess PEG was removed by centrifuged at 8,000 rpm for 10 min. The precipitates were dispersed in water for further use.

Cell culture and cytotoxicity assessment. Human cervix carcinoma cell line (HeLa) was used in our experiments. The HeLa cells are cultured in 1640 medium (GIBCO) supplemented with 10% fetal bovine serum (FBS, GIBCO) along with penicillin/streptomycin (1%, 1 g/mL). MTT assay was applied to assess cytotoxicity based on mitochondrial succinate/tetrazolium reductase system which can change yellow MTT into blue formazan and the color intensity is proportional to metabolic activity of cells. The HeLa cells were seeded in 96-well plate at a concentration of 5×10^5 cells/ mL and were cultured for 24 h. The adhered cells were then treated with varied concentrations of the as-prepared probes (0, 0.2, 0.4, 0.6, and 0.8 nM) for 24 h. The solution was replaced with 100 μL fresh medium along with 10 μL MTT (5 mg/mL) and the mixture was further cultured at 37 °C for 4 h. The dark blue formazan crystals were dissolved by 150 μL of dimethylsulfoxide and the absorbance at 490 nm were measured on a microplate reader.

SERS imaging PPi in living cells. The cells were seeded in 48-well plate at a concentration of 5×10^4 cells/mL. The plate was kept in an atmosphere of 5% CO_2 at 37 ^oC for 24 h. The free cells were removed and the adhered cells were washed with PBS (1×, pH=7.4). After that, the as-prepared probes (0.8 nM) dissolving in fresh culture medium were added and incubated with the cells for 10 h. Then, the wells were washed with PBS for 6 times to remove the probes adsorbed non-specifically. Raman imaging were performed on a Renishaw micro-Raman system coupling with a research grade Leica DMLM microscope. The images were collected using 17 mW of 633 nm (He-Ne laser) laser under a 50× objective lens. The laser was focused to roughly 1 μm spot, using scan pattern by 1 μm steps with an integration time of 0.1 s/pixel in X and Y directions. We integrated signal-to-baseline intensity from 2200 to 2300 cm^{-1} to map the signals in cellular Raman-silent region. What's more, by collecting SERS images of different "z-slices" with an interval of 2 μm, 3D images of single living cells were obtained.

RESULTS AND DISCUSSION

Preparation and characterization of the dimer probes. To enable high affinity of DPA toward AuNPs, we started this study by synthesizing DPA with a thiol moiety (termed DPASH), which can conjugate with AuNPs via Au-S bond. To do this, DPA was activated with ethylene sulfide to produce a thiol (**Scheme S1**, details are shown in Supporting Information).[32] The as-synthesized DPASH was characterized with NMR and mass spectroscopy (**Figures S1 and S2** in Supporting Information). With the DPASH in hand, we next attempted to prepare the asymmetrically functionalized PEGylated AuNPs on a glass slide (**Scheme S2**, details are shown in Supporting Information). Briefly, the 30 nm citrate-capped AuNPs were immobilized on an amino-silanized glass slide. The exposed areas of the AuNPs were reacted with the mixture of 4-MBN and DPASH at certain ratios, followed by coordinating with Zn^{2+} with high affinity. Subsequently, the glass slide was sonicated and the immobilized nanoparticles were released into solutions containing 10 μM thiolated PEGs (MW 2000). Since the MBN and DPASH molecules are inaccessible to the AuNP surface adsorbed on the glass slide, the PEGs tend to asymmetrically bound to the regions that were newly liberated by sonication. With this approach, one side of the AuNP surfaces was coated with PEGs and the other side was functionalized with the mixture of MBN and DPASH-Zn^{2+} complex at certain ratios. Note that despite the surface functionalization was confirmed by a 4-nm red shift of the maximal UV-vis spectral bands (**Figure S3** in Supporting Information), characterizing the asymmetrical surface functionalization by means of a direct tool (e.g., high-resolution transmission electron microscopy, HRTEM) remains a great challenge in the field of nano-surface chemistry.[34]

However, we can demonstrate the achievement of the asymmetrically modified AuNPs through an indirect strategy. On one hand, we hypothesized that if the AuNPs were asymmetrically functionalized with PEGs and the mixture of 4-MBN and DPASH-Zn^{2+} complex on both sides, the presence of PPi may result in the generation of nanoparticle dimers other than aggregated clusters without orientations. The TEM analysis validated our hypothesis as shown in **Figure 1c**. On the other hand, if the AuNP surfaces were randomly modified with the mixture of PEGs, MBN, and DPASH-Zn^{2+} complex, neither AuNP dimers nor clusters were formed in the presence of the same concentration of PPi (**Figure S4** in Supporting Information). This result was most likely due to the steric effect of PEG on its neighboring DPASH-Zn^{2+}, thus preventing the sandwiched complexation of DPASH-Zn^{2+}-PPi- Zn^{2+}-DPASH in the gap of the dimers. Anchoring the ligands on the AuNP surface asymmetrically is therefore essential for the nanoparticle dimerization. Moreover, the PEG can not only improve the nanoparticle water-solubility, but also facilitate the colloidal stability and biocompatibility of the probes in complex environments.[35]

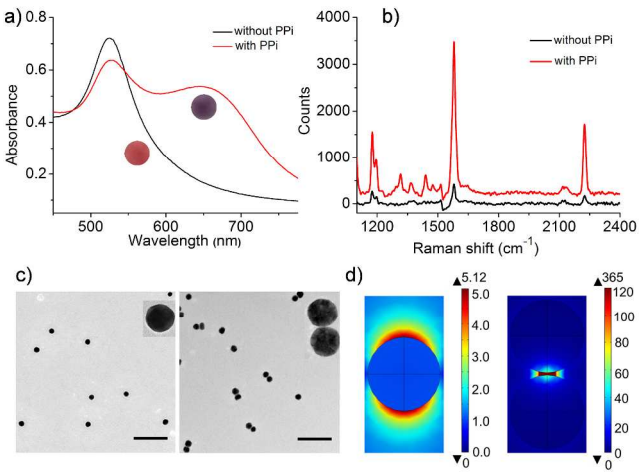

Figure 1. Feasibility of PPi detection in aqueous solution through specific PPi-triggered AuNP dimerization. a) UV-vis spectra of the asymmetrically functionalized PEGylated AuNP probes before (black line) and after (red line) addition of PPi (50 μM). Inset: corresponding colors of the AuNPs solutions before and after addition of PPi. b) SERS spectra of the AuNP probes before (black line) and after (red line) addition of PPi (50 μM). The dramatically enhanced Raman intensity reflects the formation of enhanced electromagnetic hot spots. c) TEM images of the AuNP probes in the absence or presence of PPi (50 μM). Scale bar: 200 nm. d) Near-field distributions of the normalized electric field $|\mathbf{E}|/|\mathbf{E}_{inc}|$ at the excitation laser's wavelength (633 nm) for AuNP monomer (left) and dimer (right). Much higher electromagnetic field can be seen in the gap of the dimer than that on the surface of monomer.

We next characterized the formation of AuNP dimers with several tools. When incubated the asymmetrically functionalized AuNPs (0.8 nM) with PPi (50 μM) for 40 min (the reaction time was optimized in **Figure S5** in Supporting Information), the color of the solution changed from red to purple (**Figure 1a**). The UV-vis spectrum shows that, with the decrease of the absorption peak at around 525 nm, a new peak at roughly 650 nm appeared, which is in agreement with the Mie theory, i.e., the formation of AuNP dimers leads to the decrease of transverse plasmon resonance band and the occurrence of the longitudinal interparticle plasmon coupling between the adjacent AuNPs. TEM analysis further confirmed the dimeric structures with an interparticle gap less than a few nanometers (**Figure 1c**). Therefore, significantly enhanced plasmon coupling occurs in the nanogaps (**Figure 1d**), leading to the formation of electromagnetic hot spots. As a consequence, with the addition of PPi, the Raman intensity of the MBN reporters are dramatically enhanced in comparison with that in the absence of PPi (**Figure 1b**). To validate the specific metal coordination of the dimer probes, 50 μM of PPi was added to the asymmetrically functionalized AuNP probes pretreated without Zn^{2+} or DPASH. The results showed that the colloidal solution remained red and negligible absorption spectral changes were found (**Figure S6** in Supporting Information), indicating that no AuNP dimers were formed. Therefore, only the PPi-programmed coordination with DPASH-Zn^{2+} complex can cause the formation of dimers and thus enhanced Raman scattering.

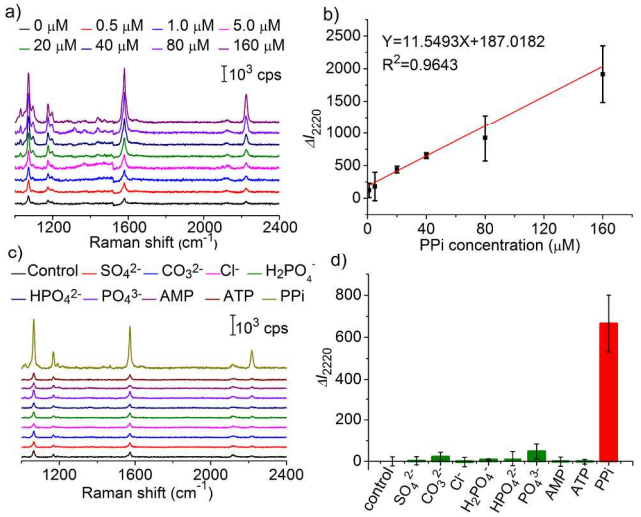

Figure 2. Sensitivity and selectivity of the AuNP probes for PPi detection in aqueous solutions. a) SERS spectra of the AuNP probes (0.8 nM) upon addition of various concentrations of PPi (0-160 μM). b) Plots of ΔI_{2220} values versus different concentrations of PPi. Error bars represent standard deviations of three independent measurements. c) SERS spectra and d) corresponding ΔI_{2220} values in the presence of 100 μM different anions. ΔI_{2220} values are the differences of Raman intensity at 2220 cm^{-1} between the testing samples and the control. To perform the Raman spectroscopic detection, the nanoparticle samples were loaded into capillaries and the measurements are carried out on a Reinshaw InVia Raman spectrometer. The error bars represent the standard deviations of three parallel samples.

Sensitivity and selectivity for PPi detection in solutions. The dramatic Raman enhancement prompted us to investigate the sensitivity and selectivity of the AuNP probes in solutions. By incubating different concentrations of PPi (0-160 μM) with the probes (0.8 nM), a concentration-dependent red-to-purple color change can be clearly observed in 40 min (**Figure S7** in Supporting Information). Higher concentrations of PPi led to more purple in color. As confirmed by the UV-vis spectra,with the increase of PPi concentration, the absorption bands at 525 nm decreased gradually, along with the red shift and absorbance increase of the newly-produced bands between 600 and 700 nm. The plots of A_{650}/A_{525} (the ratio of absorbance at 650 and 525 nm) versus various concentrations of PPi reflected the excellent concentration-dependent linearity. The limit of detection (LOD) was calculated to be ~1 μM on the basis of the calibration curve (y=0.00539x+0.2984, R^2=0.9874). Moreover, the Raman enhancement response was also dependent on the PPi concentrations. By correlating the changes of SERS intensity at 2220 cm^{-1} (ΔI_{2220}) with PPi concentrations, a calibration curve (y=11.54931x+187.0182, R^2=0.9643) was yielded, based on which the LOD was calculated to be ~0.5 μM (**Figure 2a-b**). The LOD of our method is comparable to those reported in previous studies (Table S1 in Supporting Information).

The selective response of the dimer probes were then investigated by incubating the probes with various anions (100 μM) including SO_4^{2-}, CO_3^{2-}, Cl^-, $H_2PO_4^-$, HPO_4^{2-}, PO_4^{3-}, AMP, ATP, and PPi for 40 min. The results showed that only PPi can cause the colloidal solution to change from red to purple in color, confirmed by a significant increase of the A_{650}/A_{525} value compared with those from other anions (**Figure S8** in Supporting Information). The excellent specificity was also validated by collecting the Raman spectra. As shown in **Figure 2c-d**, only PPi induced a remarkable increase of the Raman intensity. In contrast, other species caused negligible spectral changes, which was likely owing to the weak interactions between the DPASH-Zn^{2+} complex and these anions.[1,14]

PPi imaging in living cells. Encouraged by the excellent sensitivity and selectivity of the dimer probes, we attempted to detect the PPi in living cells. Commonly used Raman reporters such as malachite green isothiocyanate (MGITC) and cyanine derivatives show multiple peaks in fingerprint region (<1800 cm^{-1}),[36-38] which likely overlap with those derived from predominant cellular components particularly when they are in proximity to the probes.[31] The spectral overlap often produces background noise. To minimize this, we herein employed MBN as the Raman dye in that its nitrile moiety presents a strong and sharp single peak (2220 cm^{-1}) in the cellular Raman-silent region (1800-2800 cm^{-1}).[31] Since biospecies do not show any Raman signals in this region, the signal enhancement at 2220 cm^{-1} can specifically reflect the formation of AuNP dimers in living cells, thus indicating the presence of intracellular PPi.

We first demonstrated the in-situ formation of Raman hot spots in living cells by incubating the probes (0.8 nM) with HeLa cells for 10 h, followed by mapping the nitrile signals across several cells. As shown in **Figure 3**, the typical nitrile signals can be noticeably seen in all cells. To evaluate the specificity of the probes at live-cell level, the cells were treated with the same concentration of AuNP probes which were prepared without Zn^{2+}, and much reduced nitrile signals were observed. In order to further verify that the dimerization inside the cell was resulted from the specific binding between the Zn^{2+}-captured probe and PPi, we set another experiment as a

comparison by pretreating the cells with Mg^{2+} (0.4 mM) before incubation with the probes. Considering the high affinity of Mg^{2+} towards PPi,[1] we anticipated that the intracellular PPi could interact with the added Mg^{2+}, thus blocking the subsequent complexation between PPi and the Zn^{2+}-captured probes. As a result, the pretreatment of Mg^{2+} resulted in much reduced signals (**Figures S9** in Supporting Information).These results imply that the enhanced Raman scattering was specifically derived from the presence of PPi other than non-specific nanoparticle dimerization in cells. In addition, the excellent biocompatibility of the probes has been demonstrated with HeLa cells (details were shown in Supporting Information, **Figure S10**).

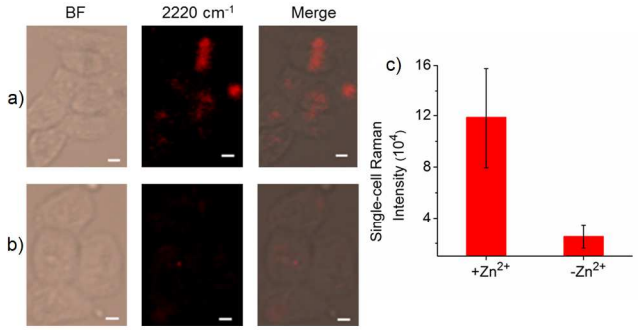

Figure 3. Bright-filed (BF) and SERS images of multiple HeLa cells which were incubated with a) the AuNP probes conjugated with the DPASH-Zn^{2+} complex and b) those pre-treated without Zn^{2+}. Scale bar: 5 μm. c) Statistics of the nitrile signals in average each cell as illustrated in a) and b).

We next verified the necessity of recording the Raman signals at the cellular Raman-silent region. MBN exhibits two major peaks at 1580 and 2220 cm^{-1}, which are assigned to the phenyl C=C and nitrile respectively. We hence performed the cellular mapping experiments with these two channels simultaneously on a confocal Raman microscope. The results in **Figure 4a** show that the Raman signals acquired in the two channels were distributed across the cell. However, the signal spots in the 2220 cm^{-1} channel (red) were less distributed than that in the 1580 cm^{-1} channel (green). We reasoned that the signals from the green channel could be attributed to both the Raman reporters and the predominant endogenous species surrounding the AuNP probes. With respect to the mapping image in the red channel, much reduced background noises were achieved because the signals were recorded from the exogenous nitrile resided in the hot spots of the dimers. The merged image shows that only the overlapping signals (point 1) can unambiguously indicate the in-situ formation of AuNP dimers and thus the location of PPi, while that remained in green (point 2) were mainly assigned to the endogenous components such as cytochrome. As confirmed by the Raman spectra, point 1 exhibits three peaks at 1520, 1580 and 2220 cm^{-1} while the peak at 2220 cm^{-1} disappeared in the spectrum of point 2 along with the marked increase of Raman intensity at 1520 cm^{-1} (the typical vibration of C–C in cytochrome) (**Figure 4b**). These results clearly demonstrate that recording the exogenous nitrile signal could be more reliable because it is completely resolved from the background noise.

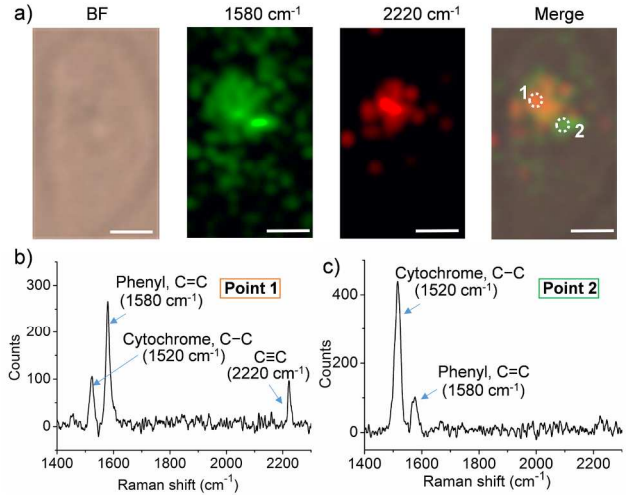

Figure 4. a) Bright-field (BF), SERS mapping images of single living cell acquired in 1580 and 2220 cm^{-1} channels and their merge. Scale bar: 5 μm. SERS spectra in b) point 1 and c) point 2.

To precisely explore the nanoparticle dimerization in living cell, three-dimensional Raman intensity mapping was performed for analyzing the enhanced nitrile signals at a depth interval of 2 μm. As shown in **Figure 5**, the exogenous nitrile Raman signals are mainly derived from the layers at the depth of 2-8 μm. At deeper depth of the cell (10 μm), very weak nitrile signals can been detected. The imaging results were confirmed by collecting the Raman spectra on each layer of the cell. The in-situ formation of AuNP dimers was finally verified by TEM analysis of 60-90 nm thick cell sections. When the probes were pre-treated without Zn^{2+}, the AuNPs were distributed in the cytosol as individuals; only the Zn^{2+}-treated probes can form dimers in cells (**Figure S11** in Supporting Information). These results reveal that the nanoparticle dimerization occurs in the cytosol other than on the cell surfaces.

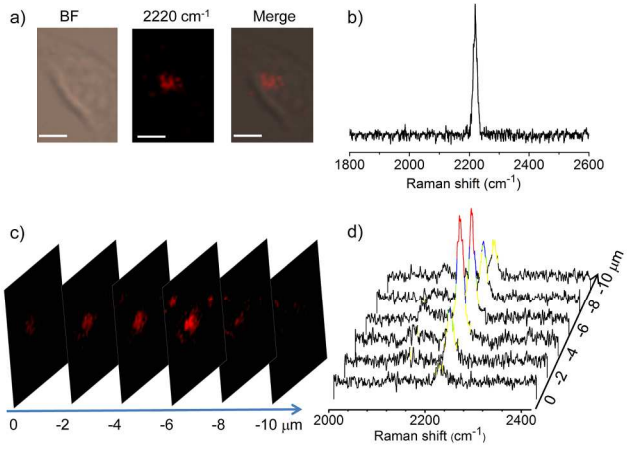

Figure 5. Three-dimensional imaging of single HeLa cell after incubating with the dimer probes for 10 h. a) Bright-field (BF), SERS image in 2220 cm^{-1} channel and their merge. Scale bar: 5 μm. b) SERS spectrum of a) in the silent region. c) SERS images taken from different layers in z-direction of the same cell. d) Typical SERS spectra of the signals in various layers.

CONCLUSION

In summary, we have reported a background-free SERS probe for highly sensitive and selective detection of PPi in both aqueous solutions and living cells. With the purpose of forming biocompatible and uniform hot spots in cells, we fabricated AuNPs whose surfaces were asymmetrically functionalized with PEG and the mixture of MBN and DPASH-Zn^{2+} complex. The specific coordination of DPASH-Zn^{2+} with PPi (2:1) enables the nanoparticle dimerization, leading to an intense Raman enhancement of MBN residing in the hot spot. More significantly, the reporter MBN exhibits a strong and sharp single peak in the cellular Raman-silent region, which can be completely resolved from the background signals. With this novel design, the distribution of PPi in living cells can be reliably monitored by the target-mediated hot-spot generation. The three-dimensional SERS imaging technique further demonstrated that the in-situ formation of Raman hot spots is specifically triggered by the intracellular target PPi. This approach can be principally applied to probe other biomolecules by only substituting the recognition ligands, opening an exciting opportunity for biosensing with high signal-to-background ratio especially in complex environments.

ASSOCIATED CONTENT

Supporting Information. Two schemes and ten additional figures. This material is available free of charge via the Internet at http://pubs.acs.org.

AUTHOR INFORMATION

Corresponding Author

*liudb@nankai.edu.cn.

Notes

The authors declare no competing financial interest.

ACKNOWLEDGMENT

This study was supported by the National Natural Science Foundation of China (21475066 and 81401463), the Tianjin Natural Science Foundation (15JCZDJC65700), the Fundamental Research Funds for Central Universities (China), and the Thousand Youth Talents Plan of China.

REFERENCES

(1) Shao, N.; Wang, H.; Gao, X.; Yang, R.; Chan, W. *Anal. Chem.* **2010**, *82*, 4628-4636.
(2) Das, P.; Bhattacharya, S.; Mishra, S.; Das, A. *Chem. Commun.* **2011**, *47*, 8118-8120.
(3) Farre, E. M.; Geigenberger, P.; Willmitzer, L.; Trethewey, R. N. *Plant. Physiol.* **2000**, *123*, 681-683.
(4) Ryan, L. M.; McCarty, D. J. *Ann. Rheum. Dis.* **1995**, *54*, 939-941.
(5) Lee, S. Y.; Yuen, K. K. Y.; Jolliffe, K. A.; Yoon, J. Y. *Chem. Soc. Rev.* **2015**, *44*, 1749-1762.
(6) Hargrove, A. E.; Nieto, S.; Zhang, T.; Sessler, J. L.; Anslyn, E. V. *Chem. Rev.* **2011**, *111*, 6603-6782.
(7) Ma, J. L.; Yin, B. C.; Wu, X.; Ye, B. C. *Anal. Chem.* **2016**, *88*, 9219-9225.
(8) Gogoi, A.; Mukherjee, S.; Ramesh, A.; Das, G. *Anal. Chem.* **2015**, *87*, 6974-6979.
(9) Chen, W. H.; Xing, Y.; Pang, Y. *Org. Lett.* **2011**, *13*, 1362-1365.
(10) Kim, S. K.; Lee, D. H.; Hong, J. I.; Yoon, J. *Acc. Chem. Res.* **2009**, *42*, 23−31.
(11) Anbu, S.; Kamalraj, S.; Jayabaskaran, C.; Mukherjee, P. S. *Inorg. Chem.* **2013**, *52*, 8294-8296.
(12) O'Neil, E. J.; Smith, B. D. *Coordin. Chem. Rev.* **2006**, *250*, 3068-3080.
(13) Su, X.; Zhang, C.; Xiao, X.; Xu, A.; Xu, Z.; Zhao, M. *Chem. Commun.* **2013**, *49*, 798-800.
(14) Ngo, H. T.; Liu, X.; Jolliffe, K. A. *Chem. Soc. Rev.* **2012**, *41*, 4928-4965.
(15) Zhang, J. F.; Kim, S.; Han, J. H.; Lee, S. J.; Pradhan, T.; Cao, Q. Y.; Lee, S. J.; Kang, C.; Kim, J. S. *Org. Lett.* **2011**, *13*, 5294-5297.
(16) Hai, Z.; Bao, Y.; Miao, Q.; Yi, X.; Liang, G. *Anal. Chem.* **2015**, *87*, 2678-2684.
(17) Zhu, W.; Huang, X.; Guo, Z.; Wu, X.; Yu, H.; Tian, H. *Chem. Commun.* **2012**, *48*, 1784-1786.
(18) Wen, J.; Geng, Z.; Yin, Y.; Zhang, Z.; Wang, Z. *Dalton. Trans.* **2011**, *40*, 1984-1989.
(19) Mesquita, L. M.; Andre, V.; Esteves, C. V.; Palmeira, T.; Berberan-Santos, M. N.; Mateus, P.; Delgado, R. *Inorg. Chem.* **2016**, *55*, 2212-2219.
(20) Lee, H. N.; Xu, Z. C.; Kim, S. K.; Swamy, K. M. K.; Kim, Y.; Kim, S. J.; Yoon, J. Y. *J. Am. Chem. Soc.* **2007**, *129*, 3828-3829.
(21) Schlucker, S. *Angew. Chem., Int. Ed.* **2014**, *53*, 4756-4795.
(22) Wang, Y.; Yan, B.; Chen, L. *Chem. Rev.* **2013**, *113*, 1391-1428.
(23) Guerrini, L.; Graham, D. *Chem. Soc. Rev.* **2012**, *41*, 7085-7107.
(24) Xu, L.-J.; Lei, Z.-C.; Li, J.; Zong, C.; Yang, C. J.; Ren, B. *J. Am. Chem. Soc.* **2015**, *137*, 5149-5154.
(25) Zheng, Y.; Soeriyadi, A. H.; Rosa, L.; Ng, S. H.; Bach, U.; Justin Gooding, J. *Nat. Commun.* **2015**, *6*, 8797-8804.
(26) Huang, Y. F.; Zhang, M.; Zhao, L. B.; Feng, J. M.; Wu, D. Y.; Ren, B.; Tian, Z. Q. *Angew. Chem., Int. Ed.* **2014**, *53*, 2353-2357.
(27) Li, J.; Zhu, Z.; Zhu, B.; Ma, Y.; Lin, B.; Liu, R.; Song, Y.; Lin, H.;Tu, S.; Yang, C. *Anal. Chem.* **2016**, *88*, 7828-7836.
(28) Wu, J.; Liang, D.; Jin, Q.; Liu, J.; Zheng, M.; Duan, X.; Tang, X. *Chem. Eur. J.* **2015**, *21*, 12914-12918.
(29) Chen, Y.; Ren, J. Q.; Zhang, X. G.; Wu, D. Y.; Shen, A. G.; Hu, J. M. *Anal. Chem.* **2016**, *88*, 6115-6119.
(30) Kong, K. V.; Lam, Z.; Goh, W. D.; Leong, W. K.; Olivo, M. *Angew. Chem., Int. Ed.* **2012**, *51*, 9796-9799.
(31) Hong, S.; Lin, L.; Xiao, M.; Chen, X. *Curr. Opin. Chem. Biol.* **2015**, *24*, 91-96.
(32) Kurosaki, H.; Tawada, T.; Kawasoe, S.; Ohashi, Y.; Goto, M. *Bioorg. Med. Chem. Lett.* **2000**, *10*, 1333-1337.
(33) Turkevich, J.; Stevenson, P. C.; Hillie, J. *Discuss. Faraday. Soc.* **1951**, *11*, 55-75.
(34) Sardar, R.; Heap, T. B.; Shumaker-Parry, J. S. *J. Am. Chem. Soc.* **2007**, *129*, 5356-5357.
(35) Hayashi, K.; Nakamura, M.; Miki, H.; Ozaki, S.; Abe, M.; Matsumoto, T.; Ishimura, K. *Chem. Commun.* **2013**, *49*, 5334-5336.
(36) Lane, L. A.; Qian, X.; Nie, S. *Chem. Rev.* **2015**, *115*, 10489-10529.
(37) Qian, X.; Emory, S. R.; Nie, S. *J. Am. Chem. Soc.* **2012**, *134*, 2000-2003.
(38) Samanta, A.; Maiti, K. K.; Soh, K. S.; Liao, X.; Vendrell, M.; Dinish, U. S.; Yun, S. W.; Bhuvaneswari, R.; Kim, H.; Rautela, S.; Chung, J.; Olivo, M.; Chang, Y. T. *Angew. Chem., Int. Ed.* **2011**, *50*, 6089-6092.

Insert Table of Contents artwork here